iScience

CellPress
OPEN ACCESS

Article

Understanding COVID-19 progression with longitudinal peripheral blood mononuclear cell proteomics: Changes in the cellular proteome over time

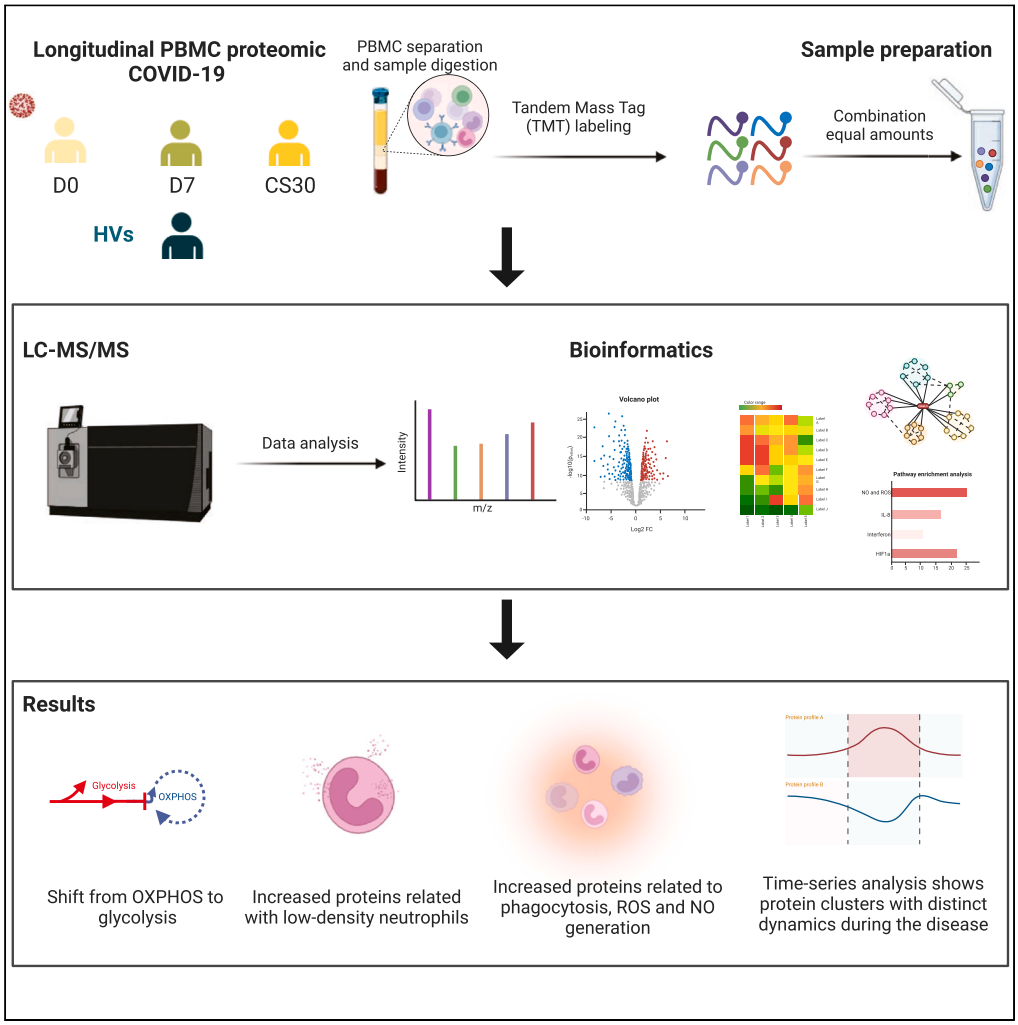

Giuseppe Gianini Figueirêdo Leite, Milena Karina Colo Brunialti, Paula M. Peçanha-Pietrobom, ..., Graziella E. Ronsein, Alexandre Keiji Tashima, Reinaldo Salomão

rsalomao@unifesp.br

Highlights

Longitudinal PBMC proteomic profiles differs according to COVID-19 patients' outcomes

Patients present a switch from OXPHOS to glycolysis with enriched PPP abundance

PPI reveals modules enriched to neutrophil degranulation and antimicrobial response

Time-series analysis shows protein clusters with distinct dynamics during the disease

Figueirêdo Leite et al., iScience *26*, 107824
October 20, 2023
https://doi.org/10.1016/j.isci.2023.107824

iScience

CellPress
OPEN ACCESS

Article

Understanding COVID-19 progression with longitudinal peripheral blood mononuclear cell proteomics: Changes in the cellular proteome over time

Giuseppe Gianini Figueirêdo Leite,[1] Milena Karina Colo Brunialti,[1] Paula M. Peçanha-Pietrobom,[1] Paulo R. Abrão Ferreira,[1] Jaquelina Sonoe Ota-Arakaki,[2] Edecio Cunha-Neto,[3] Bianca Lima Ferreira,[1] Graziella E. Ronsein,[4] Alexandre Keiji Tashima,[5] and Reinaldo Salomão[1,6,*]

SUMMARY

The clinical presentation of COVID-19 is highly variable, and understanding the underlying biological processes is crucial. This study utilized a proteomic analysis to investigate dysregulated processes in the peripheral blood mononuclear cells of patients with COVID-19 compared to healthy volunteers. Samples were collected at different stages of the disease, including hospital admission, after 7 days of hospitalization, and 30 days after discharge. Metabolic pathway alterations and increased abundance of neutrophil-related proteins were observed in patients. Patients progressing to critical illness had significantly low-abundance proteins in the pentose phosphate and glycolysis pathways compared with those presenting clinical recovery. Important biological processes, such as fatty acid concentration and glucose metabolism disorder, remained altered even after 30 days of hospital discharge. Temporal proteomic changes revealed distinct pathways in critically ill and non-critically ill patients. Our study emphasizes the significance of longitudinal cellular proteomic studies in identifying disease progression-related pathways and persistent protein changes post-hospitalization.

INTRODUCTION

The coronavirus disease 2019 (COVID-19) pandemic has caused an unparalleled worldwide disaster, with millions of lives lost, public health systems in shock, and economic and social devastation.[1] The causative pathogen emerged in Wuhan, China, and was named severe acute respiratory syndrome coronavirus 2 (SARS-CoV-2), which is the third coronavirus to cause severe respiratory disease in humans after SARS-CoV and Middle East respiratory syndrome coronavirus.[2]

The clinical presentation of COVID-19 is heterogeneous, varying from asymptomatic (or presymptomatic), mild, moderate, severe, to critical disease.[3–6] Patients who survive continue to exhibit COVID-19-related symptoms even months after discharge, such as fatigue, cognitive dysfunction, and shortness of breath.[7]

Mass spectrometry (MS)-based proteomics, mostly focused on plasma, serum, and bronchoalveolar lavage fluid, has been used as a powerful tool to elucidate a broad range of dysregulated biological processes in patients with COVID-19.[8–12] However, few studies have been conducted using patient's cells, such as peripheral blood mononuclear cells (PBMCs).[13,14] PBMCs are composed of several classes of immune cells, such as T cells, B cells, monocytes, dendritic cells, natural killer cells, and a cellular subclass of neutrophils, low-density neutrophils (LDNs), which are also known as myeloid-derived polymorphonuclear neutrophil suppressor cells.[15,16] This variety of cells may provide a more comprehensive picture of the immune system status than circulating serum or plasma.[17]

In this study, a tandem mass tag (TMT)-based quantitative proteomic approach combined with bioinformatics analyses was used to investigate the presence of altered proteins related to different dysregulated pathways and biological processes in patients with COVID-19. We focused on moderately ill patients admitted to the hospital wards and presenting either (1) clinical recovery and short hospitalization or (2) clinical deterioration and need for intensive care unit (ICU) support. Samples were obtained prospectively during the clinical course of the disease and after hospital discharge, thus gaining the opportunity to investigate proteome changes in the early days of the disease and after clinical recovery in patients with different clinical outcomes.

[1]Division of Infectious Diseases, Escola Paulista de Medicina, Universidade Federal de São Paulo, São Paulo, Brazil
[2]Division of Respiratory Diseases, Escola Paulista de Medicina, Universidade Federal de São Paulo, São Paulo, Brazil
[3]Laboratory of Immunology, Heart Institute, University of São Paulo School of Medicine, São Paulo, Brazil
[4]Department of Biochemistry, Chemistry Institute, University of São Paulo, SP, Brazil
[5]Department of Biochemistry, Escola Paulista de Medicina, Universidade Federal de São Paulo, São Paulo, Brazil
[6]Lead contact
*Correspondence: rsalomao@unifesp.br
https://doi.org/10.1016/j.isci.2023.107824

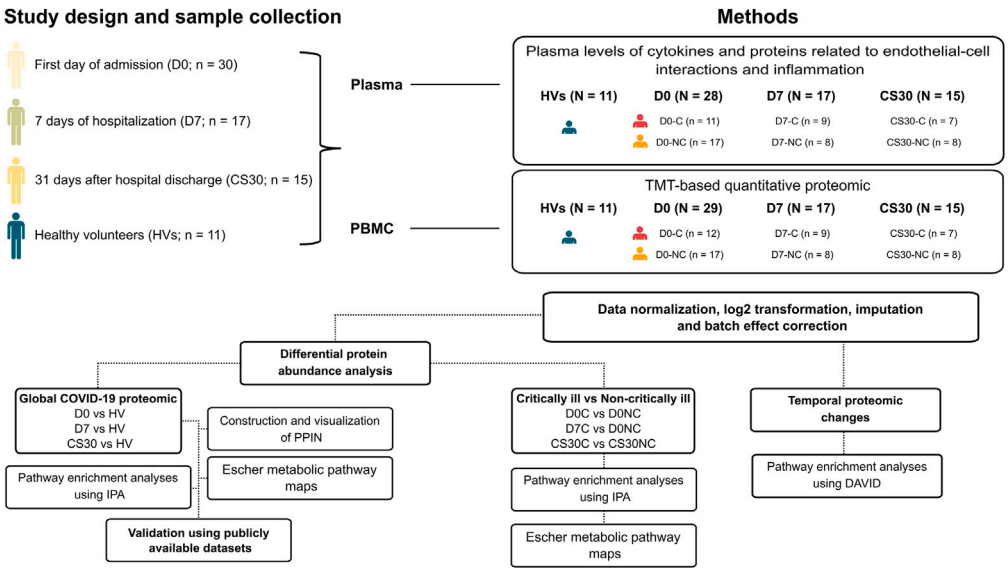

Figure 1. Experimental workflow

Scheme of the cohort, timing of the blood sample collection, and methods. Note: proteomic data were subjected to iterative outlier removal using the molecular degree perturbation (MDP) web tool.[19] After MDP analyses, one patient was detected as an outlier and removed from all subsequent analyses (Figure S1).

RESULTS

Clinical and epidemiological features of the study participants

The 29 patients with COVID-19 included in the proteomic analysis are part of a cohort of COVID-19 patients admitted to the hospital wards and presenting distinct clinical outcomes.[18] The mean age of the patients was 69 years. The majority of the patients were male (n = 19, 65%). The mean duration of symptoms before admission was 6.7 $\pm$ 3.1 days. The main symptoms were fever (n = 20; 69%), cough (n = 20; 69%), shortness of breath (n = 18; 62.1%), and diarrhea (n = 7; 24.1%). The mean of hospitalization days was 19.1 $\pm$ 20.8. Among the 29 patients, 12 (41.4%) progressed to clinical deterioration and critical illness, and 17 (58.6%) presented clinical recovery and were classified as non-critical. At the time of the first sampling (D0), all patients were admitted to the ward, and 16 (55.2%) required supplementary oxygen. At the time of the second sampling (D7, n = 17), 9 (52.9%) were admitted to the ward, and 8 (47.1%) were admitted to the ICU. Among the patients, three died during hospitalization.

At admission, patients presenting with deteriorating clinical courses showed elevated levels of neutrophils, neutrophil-lymphocyte ratio, creatinine, and C-reactive protein compared with patients with clinical recovery and short hospitalization. Epidemiologic, clinical, and routine laboratory data of the 29 patients with COVID-19 are shown in Table S1.

Global COVID-19 proteomic quantification

Prospective sample collection was carried out during hospitalization and after hospital discharge, resulting in a single visit per patient. The patient samples were stratified according to the collection day and the clinical course observed during hospitalization. An overview of the study, including the number of samples collected and the methodology employed, is presented in Figure 1.

TMT labeling and an LC-MS/MS strategy were applied to quantify differentially abundant proteins (DAPs) among patients with COVID-19, stratified according to the day of blood sampling and clinical outcomes (critical and non-critical), and healthy volunteers (HVs). A total of 2,196 proteins were found in the 73 samples of the 15 TMT batches. When restricted to proteins quantified in at least 50% of samples and after outlier removal, this number dropped to 72 samples and 1452 proteins identified with an average of 1283 proteins per sample (Figure S2; Table S2).

This proteomic analysis of PBMCs provides a comprehensive scope of the systemic host response to SARS-CoV-2 infection. Compared with HVs, patients with COVID-19 showed considerable differences in proteomic profiles (Figure 2). In patients with COVID-19, 348 proteins as DAPs were identified at D0 (169 low- and 179 high-abundance proteins) (Figure 2A; Table S3), 249 DAPs were identified at D7 (110 low- and 139 high-abundance proteins) (Figure 2B; Table S4), and 109 DAPs were identified at CS30 (40 low- and 69 high-abundance proteins) (Figure 2C; Table S5). A total of 34 common proteins were found in these three follow-up samples (Figure 2D; Table S6), of which 33 had the same direction (Figure 2F). These proteins were involved in the tricarboxylic acid (TCA) cycle, oxidative phosphorylation (OXPHOS), and carbon metabolism.

IPA enrichment analysis identified eight canonical pathways significantly enriched in D0, eight enriched canonical pathways in D7, and two enriched canonical pathways in CS30 (Figure 2E). The TCA cycle and OXPHOS were predicted to be decreased in contrast to macrophage

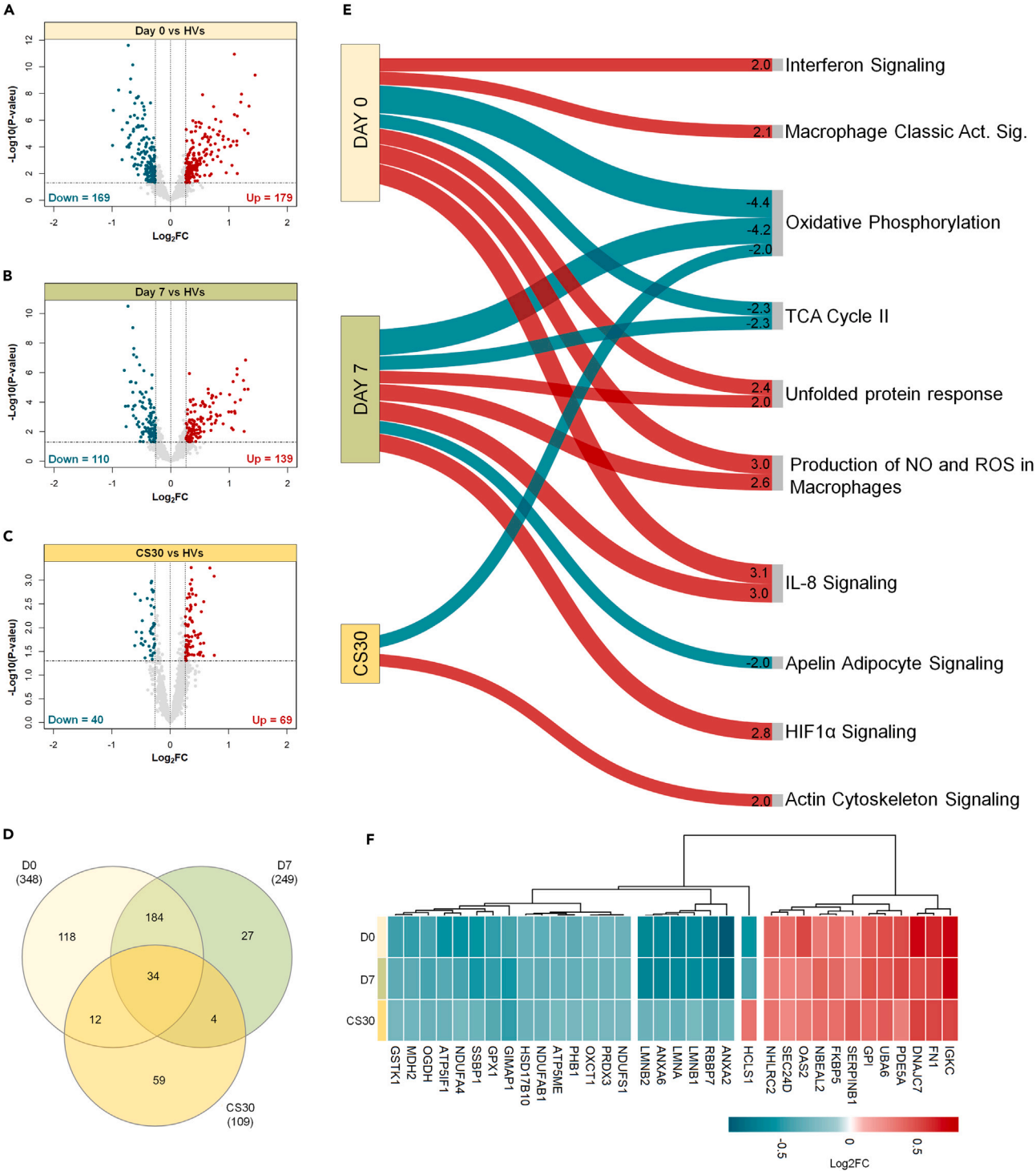

Figure 2. The overall distribution of differentially abundant proteins (DAPs)

(A–C) Volcano plots of DAPs at (A) D0 (n = 29) compared with healthy volunteers (HVs) (n = 11), (B) D7 (n = 17) compared with HVs (n = 11), and (C) CS30 (n = 15) compared with HVs (n = 11). Cyan dots represent low-abundance proteins, red dots represent high-abundance proteins, and gray dots represent proteins that were not differentially abundant.

(D) Venn diagram showing the overlap between three lists of DAPs.

Figure 2. *Continued*

(E) Sankey diagram showing the results of the IPA canonical pathway analysis. Red lines represent a canonical pathway predicted to be significantly increased, and cyan lines represent a canonical pathway predicted to be significantly decreased (IPA *Z* score ≥ 2 or ≤ -2 with a B-H q-value <0.05).

(F) The heatmap of 34 common DAPs at D0, D7, and CS30. The color scale illustrates the relative level of DAP: red, higher than the HVs, and cyan, below the reference HVs.

activation, nitric oxide (NO) and reactive oxygen species (ROS) production in macrophages, and interleukin (IL)-8 signaling, which were predicted to be increased. These changes were common at D0 and D7. Noteworthy, actin cytoskeleton signaling was only enriched (predicted increase) at CS30. Additionally, 118 diseases or functional annotations were enriched in at least one time point (Table S7). Some of them remained with the same direction of alteration during hospitalization (D0 and D7) and 30 days after discharge, such as fatty acid concentration, glucose metabolism disorder, mitochondria transmembrane potential, insulin resistance, and apoptosis. Others were predicted to be increased at D0 and D7 and decreased at CS30, such as activation of blood platelets, blood coagulation, chemotaxis of myeloid cells, and phagocytosis of cells (Figure S3).

Principal component analysis (PCA) of DAPs segregated patients with COVID-19 and HVs at D0 (Figure 3A). This segregation remained at D7, and it was not possible to observe a clear separation between the two groups at CS30 (Figures S4A and S4B). Additionally, DAP lists were investigated in the PPIN (Figure S5). Based on the Markov clustering analysis, four densely connected regions (modules) were identified, including a module enriched for the generation of precursor metabolites/energy and TCA cycle/respiratory electron transport, a module enriched for the processing of capped intron-containing pre-mRNA and mRNA processing, and two modules enriched to myeloid leukocyte activation, neutrophil degranulation, and antimicrobial humoral response (Figure 3B). Noteworthy, these two modules contain proteins with increased abundance which are related to the neutrophil biological functions, indicating the presence of co-purified LDNs in the PBMCs fraction of patients' samples, which has been previously reported in patients with COVID-19 and sepsis.[20–22]

Upon a specific analysis of glycolysis, pentose phosphate pathway (PPP), and TCA cycle using Escher metabolic pathway maps, high-abundance proteins were found in glycolysis and PPP in patients at D0, whereas the TCA enzymes, isocitrate dehydrogenase, succinate dehydrogenase, 2-oxoglutarate dehydrogenase, succinyl-CoA ligase, and malate dehydrogenase mitochondrial, had low-abundance compared with HVs (Figure 3C). A similar profile was found at D7, while an almost complete return to homeostasis was found at CS30 (Figures S6A and S6B).

Distinctive molecular signature for patients with COVID-19 progressing to critical disease (critically ill) and those with clinical recovery (non-critically ill)

The patients were divided into two groups: critically ill and non-critically ill patients. For each day of sampling, an analysis was performed to assess the differences between patients with distinct clinical courses: D0-critical (n = 12) versus D0-non-critical (n = 17), D7-critical (n = 9) versus D7-non-critical (n = 8), and CS30-critical (n = 7) versus CS30-non-critical (n = 8). The PCA plot, which illustrates the differences and similarities between the different days and outcomes, can be found in Figure S7. A total of 195 proteins as DAPs were identified in D0-critical patients compared with D0-non-critical patients (146 low- and 49 high-abundance proteins) (Figure 4A; Table S8), 215 DAPs were identified at D7 (123 low- and 92 high-abundance proteins) (Figure 4B; Table S9), and 225 DAPs were identified at CS30 (78 low- and 147 high-abundance proteins) (Figure 4C; Table S10). Additionally, six proteins consistently showed differing abundances in critically ill patients compared to non-critical patients across all three examined time points. These proteins comprise unconventional myosin-Ig (MYO1G), X-ray repair cross-complementing protein 6 (XRCC6), 14-3-3 protein gamma (YWHAG), GTP-binding nuclear protein Ran (RAN), neurogranin (NRGN), and 3′-5′ RNA helicase YTHDC2 (YTHDC2), as detailed in Table S11.

IPA enrichment analysis identified 10 canonical pathways in D0-critical patients compared with D0-non-critical patients, and all were predicted to be significantly decreased. Unexpectedly, only two enriched canonical pathways were found in D7-critical patients: one was found to be decreased, and the other was found to be increased. Interestingly, 31 enriched canonical pathways were found at CS30, and the majority significantly increased in critical patients. Figure 4D represents pathways with unique proteins enriched in each pathway; among those with redundant proteins enriched, the pathway most relevant to the biology of SARS-CoV-2 infection was chosen (Table S12).

Escher metabolic pathway maps revealed that the main metabolic changes between critical and non-critical samples were found at D0, with significant low-abundance proteins involved in the PPP and glycolysis pathway in critical patients (Figure S8A). These changes are not maintained over time (Figures S8B and S8C).

Temporal proteomic changes

A time-series soft clustering analysis considering the clinical outcomes (critical and non-critical) and day-specific proteomics was performed using Mfuzz to explore protein abundance patterns during the clinical course of hospitalized patients with COVID-19. This analysis revealed the presence of 5 clusters. Only 4 clusters presented enriched pathways. Cluster 1, containing 143 core proteins involved in neutrophil degranulation and the innate immune system, showed a continuous high-abundance during the clinical course of hospitalization and levels similar to those of the HVs after discharge from the hospital (Figure 5A; Table S13). Cluster 2, containing 143 core proteins, was enriched for platelet functions and neutrophil degranulation and presented high-abundance in critical patients, regardless of the day of sample collection, whereas non-critical patients were similar to the HVs (Figure 5B; Table S14). Cluster 3, containing 140 core proteins, showed low-abundance in patients with COVID-19 at D0 and a rising trend of protein abundance during follow-up, which was similar to the HVs in CS30 samples. This cluster was enriched for the metabolism of RNA and IL-12 signaling pathways (Figure 5C; Table S15). Cluster 4 showed no enriched pathways

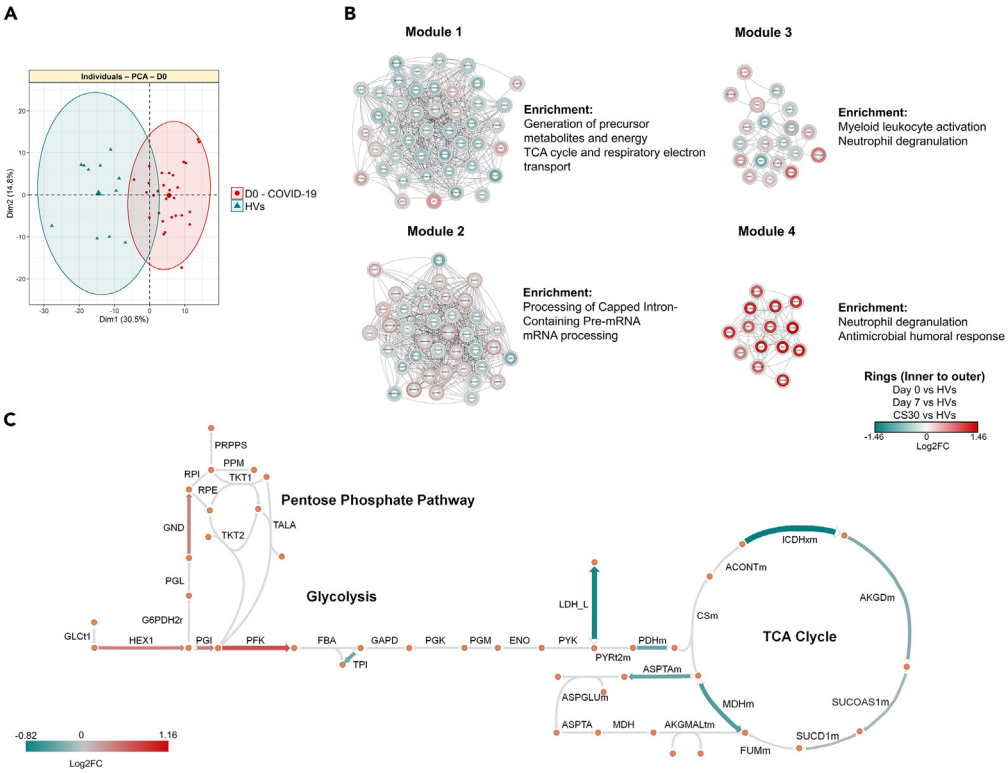

Figure 3. Protein abundance, densely connected regions, and glycolysis metabolism in patients with COVID-19

(A) Principal component analysis of 348 differentially altered proteins identified from patients with COVID-19 at D0 compared with HVs. The ellipses represent 95% confidence intervals around the centroid of each data cluster. Each dot and triangle represent one sample. Cyan represents HVs samples, and red represents COVID-19 samples.

(B) Protein-protein interaction network (PPIN) modules in COVID-19. Cyan rings represent the low-abundance proteins, and red rings represent the high-abundance proteins. The inner rings represent D0 abundance, the center rings represent D7 abundance, and the outer rings represent CS30 abundance. The enriched pathways generated through the STRING enrichment are shown separately for each module (false discovery rate-corrected p value <0.05).

(C) Metabolic map visualization for glycolysis, pentose phosphate pathway (PPP), and tricarboxylic acid (TCA) cycle. The scale represents DAPs from patients at D0 (n = 29) compared with HVs (n = 11).

(Table S16). Cluster 5 (77 core proteins) showed high-abundance in non-critical patients and low-abundance in critical patients (regardless of the day of sample collection) and was enriched for eukaryotic translation elongation and peptide chain elongation (Figure 5D; Table S17).

Comparison with other human proteomic datasets

A public dataset of PBMCs from patients with COVID-19 was reanalyzed to validate our results related to metabolism and LDNs. Based on DAPs, IPA, and PPIN module analyses, 42 metabolism-related and 24 LDN-related proteins were selected. These proteins were manually curated for their biological functions using the UniProt (https://www.uniprot.org/). Compared with the PBMCs dataset from Carapito et al.,[14] 11 metabolism-related proteins were found in common, 8 with high-abundance (UGP2, PFKP, LDHA, PGD, PYGL, GPI, HK3, and ACLY) and three with low-abundance (GLUD1, COX4I1, and COX7A2). Regarding LDN-related proteins, 10 proteins were found in common, all with high-abundance (LTF, MPO, CTSG, ITGAM, MMP9, BPI, PRTN3, CEACAM8, LCN2, and S100A12) (Figures S9A and S9B).

Plasma levels of cytokines and proteins related to endothelial-cell interactions and inflammation

Since PBMCs are a subset of the peripheral blood cells and represent a source and target of circulating cytokines, the plasma levels of these mediators were evaluated in patients with COVID-19 and HVs. The findings showed that patients with COVID-19 showed increased levels of cytokines and proteins related to endothelial-cell interactions and inflammation, which is consistent with earlier reports.[23,24]

Overall, 12 analytes were differentially abundant in plasma from patients with COVID-19 versus HVs at D0, including increased levels of cytokines (IL-6, IL-8, IL-10, and IL-18), soluble intercellular adhesion proteins (s-ICAM-1, sVCAM-1, and P-selectin), a mediator modulating vascular response (GDF-15) and levels of neutrophil proliferation and degranulation marks (NGAL and MPO). Nine mediators were altered at D7 and six at CS30. IL-6 and IL-10 remained altered at D0 and D7, while GDF-15, sICAM-1, MPO, P-selectin, IL-8, and IL-18 were found significantly altered at the three different time points. Critical patients at D0 showed increased MYO, NGAL, sVCAM-1, and GM-CSF

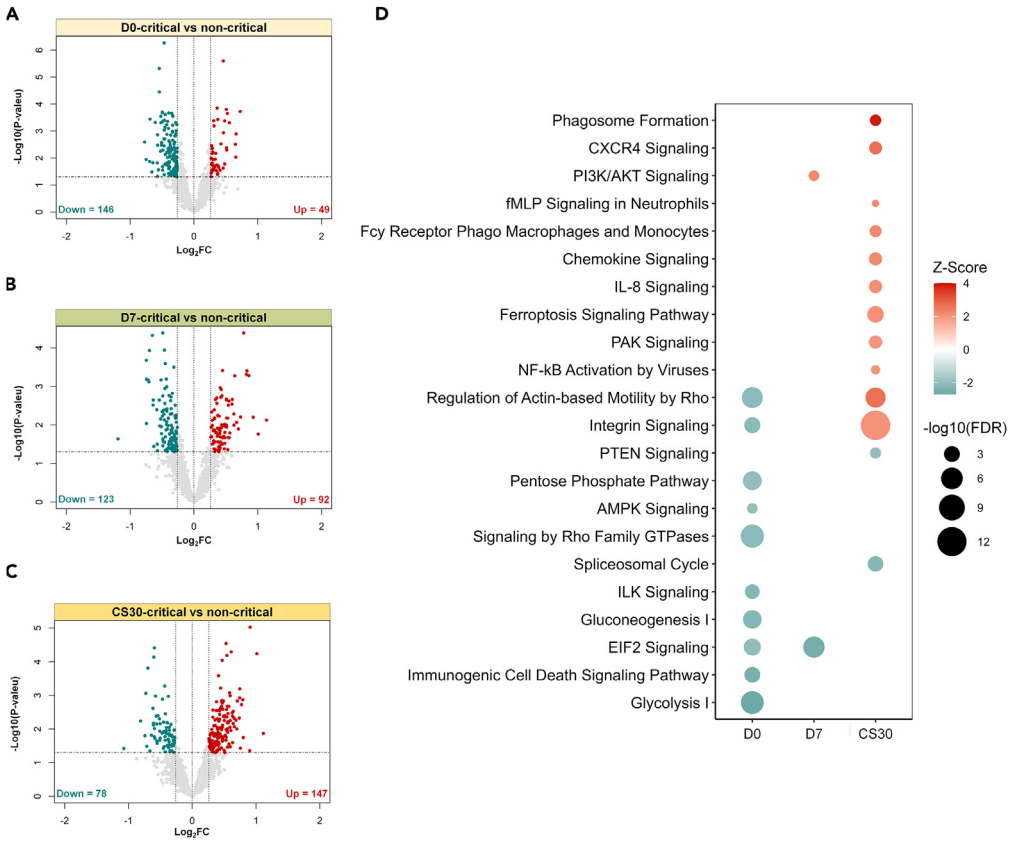

Figure 4. Distinctive response for critically ill and non-critically ill patients

(A–C) Volcano plots of DAPs in (A) D0-critical (n = 12) versus D0-non-critical (n = 17), (B) D7-critical (n = 9) versus D7-non-critical (n = 8), and (C) CS30-critical (n = 7) versus CS30-non-critical (n = 8) patients. Cyan dots represent low-abundance proteins, red dots represent high-abundance proteins, and gray dots represent proteins that were not differentially abundant.

(D) Dot plot showing the IPA canonical pathway analysis results. Red dots represent a canonical pathway predicted to be significantly increased, and cyan dots represent a canonical pathway predicted to be significantly decreased (IPA *Z* score ≥ 2 or ≤ -2 with a B-H q-value <0.05).

compared with non-critical patients. Critical patients at D7 showed increased levels of GDF-15, MYO, sICAM-1, sVCAM-1, IL-6, and IL-17A, and IL-6 and IL-9 remained high in critically ill patients even after 30 days of discharge (Table S18).

DISCUSSION

In order to understand the diverse responses to SARS-CoV-2 infection, it is crucial to employ high-resolution techniques and well-characterized clinical cohorts. Using TMT-based quantitative proteomics and bioinformatics analysis, we present the first PBMC proteomic study of a cohort of COVID-19 patients admitted to hospital wards, with diverse outcomes, and including samples throughout the disease course and after discharge.

Broad dysregulation of proteins related to metabolic machinery may represent either an antiviral response or viral-mediated disruption of host transcripts and translation.[25] Previous omics studies have reported altered metabolic pathways during SARS-CoV-2 infection.[26–29] These results are consistent with those of our study, which showed a switch from OXPHOS to glycolysis at D0 and D7 with a "truncated" TCA cycle, similar to that observed in the Warburg effect, in which it supports defense against bacterial and viral infection.[30,31] These cellular metabolic changes drive an important cellular immune response. For example, a switch to glycolysis is related to the sufficient generation of adenosine triphosphate (ATP) and biosynthetic intermediates to perform their specific effect functions,[32,33] including phagocytosis and antimicrobial response, which are predicted to be increased in this study.

Metabolic pathways, such as those related to fatty acid metabolism, OXPHOS, glucose metabolism disorder, and insulin resistance, remained altered during the hospital stay (D0 and D7 samples) and even after hospital discharge (CS30 samples) compared with HVs. Proteins involved in the TCA cycle (MDH2 and OGDH) and mitochondrial electron transport chain and ATP synthesis (NDUFA4, NDUFAB1, NDUFS1, ATP5IF1, and ATP5ME) were found in low-abundance 30 days after discharge. This finding is consistent with previous reports on post-acute sequelae of COVID-19 or long COVID-19 showing a chronic and self-perpetuating metabolically imbalanced non-resolving condition defined by mitochondrial dysfunction, in which ROS drive inflammation and a switch to glycolysis.[34,35]

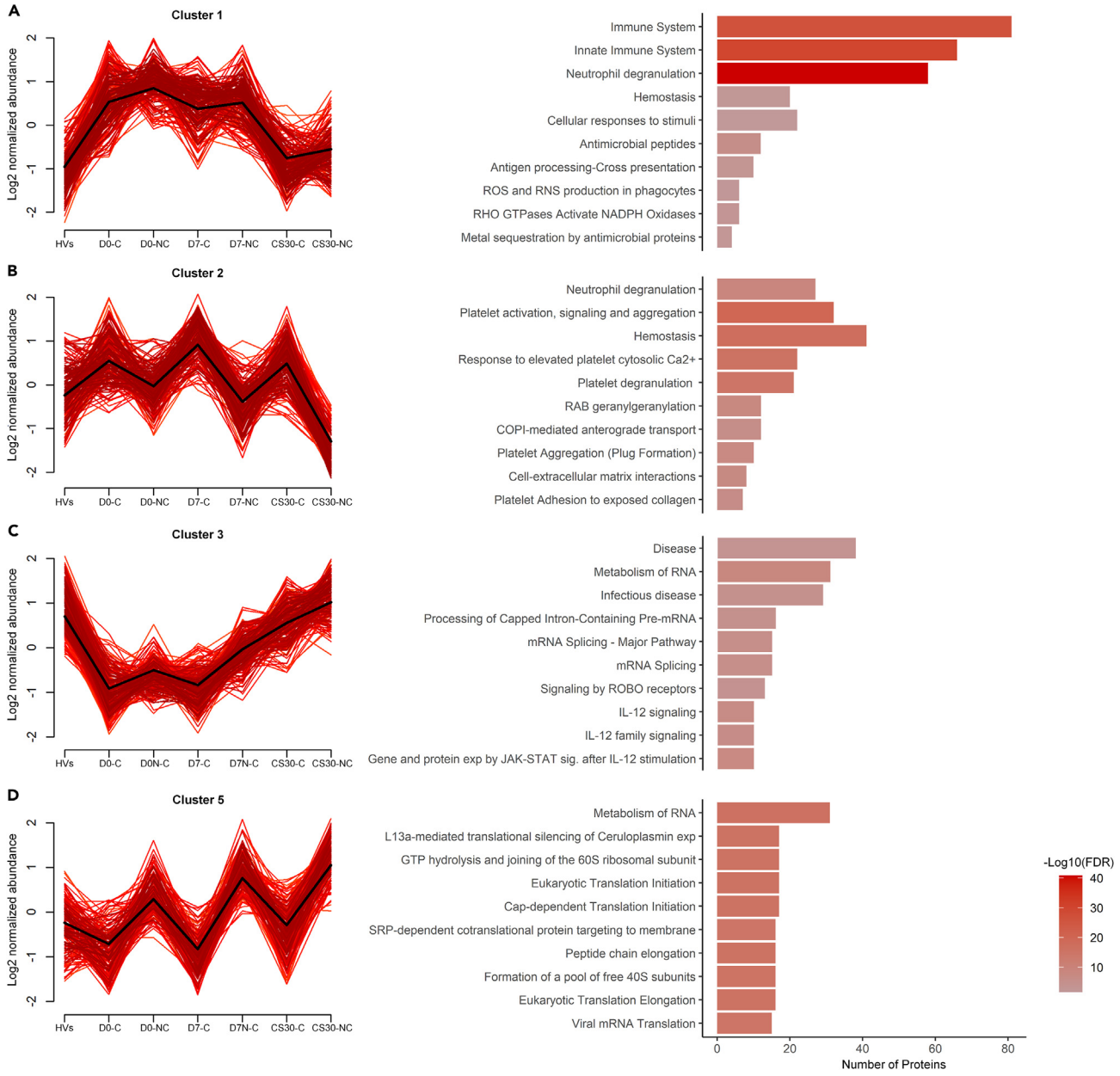

Figure 5. Soft clustering analysis of the proteomic abundance pattern

Trend analysis of cluster proteins with similar abundance patterns according to their temporal profiles and the top 10 enriched REACTOME pathways. (A) cluster 1, (B) cluster 2, (C) cluster 3, (D) cluster 5.

Interestingly, patients progressing to critical illness showed a marked difference in metabolic pathways compared with those not progressing to clinical deterioration already at hospital admission. Thus, non-critical patients showed greater protein abundance in the glucose and PPP pathways than critical patients, whereas the TCA cycle was equivalently altered in both groups. The increased abundance of PPP-related proteins was associated with the supply of nicotinamide adenine dinucleotide phosphate to drive ROS production, antimicrobial response, and defense against acute oxidative stress.[36,37] On the other hand, the decrease in PPP-related proteins could induce oxidative damage, cell apoptosis, and inflammatory cytokine release.[38,39] This finding is consistent with previous reports indicating that PPP-related protein deficiencies may be associated with poor outcomes in patients with COVID-19.[40,41] In contrast, CS30 critically ill patients presented several pathways predicted to be increased when compared to non-critically ill. Patients with deteriorating clinical courses received critical supportive therapy tailored to their needs, including ventilatory support and dialysis. In addition to more invasive supportive therapy, critically ill patients had a significantly longer hospital stay, with an average of 33.91 (25.93) days, compared to non-critically ill patients, who stayed an average of

8.6 (3.8) days. Consequently, the severity of the disease and the supportive interventions during the hospital stay may contribute to the post-discharge differences observed between the two groups.

Changes in the abundance of metabolism-related proteins were also highlighted in the time-series soft clustering analysis. Cluster 3 was enriched to splicing processes and cap processing and exhibited low-abundance in patients with COVID-19 at D0 and a rising trend of protein abundance during follow-up. The same pattern was observed for the whole cohort of patients. In contrast, cluster 5, more related to protein metabolism (eukaryotic translation elongation and peptide chain elongation), exhibited differences between critical and non-critical patients, with high-abundance in non-critical patients, which was sustained 30 days after hospital discharge. This pattern is similar to what is known as "host-shutoff," which is related to the remodeling of host gene expression and protein synthesis, leading to disrupted splicing and accelerated degradation of cytosolic cellular mRNAs and facilitating the viral takeover of the mRNA pool in infected cells, thus increasing translation of viral proteins, promoting escape, and disrupting innate immune pathways.[42–44]

Additionally, we found many proteins enriched for neutrophil-related processes, such as azurophilic granule proteins, neutrophil granule proteins, neutrophil elastase, and neutrophil collagenase, indicating the presence of LDNs co-purified with PBMCs, as previously reported.[20–22] Recent studies have suggested different functions of these cells, such as a high capacity to generate ROS, increased phagocytic capacity, elevated neutrophil extracellular trap formation, and association with the suppression of T cell function and proliferation.[15,45] The increase in the number of LDNs may be associated with the severity of infectious diseases, such as COVID-19 and sepsis.[22,46,47] This is reinforced in our temporal analysis results (cluster 2), in which it was possible to visualize a trend for neutrophil degranulation and platelet functions with high-abundance in critical patients, regardless of the day of sample collection.

Furthermore, the presence of LDNs in PBMCs may be associated with emergency hematopoiesis/granulopoiesis in these patients,[48] which is in agreement with the increase in the abundance of multiple inflammatory signals, such as IL-6, IL-8, IL-10, and G-CSF, which prolong the lifespan of neutrophils and infiltration[15,47,49] as well as high levels of neutrophil proliferation and degranulation marks[50,51] and leukocytes rolling mediators over vascular surfaces.[52] Additionally, the results of plasma biomarkers, particularly at D0 and D7, align with the state of inflammation and alterations of metabolic pathways observed in the proteome of PBMCs from these patients. These findings are consistent with those reported by Xiao et al.,[53] who showed that reprogrammed host metabolism was tightly linked to the burst of proinflammatory cytokines. Moreover, the presence of inflammatory markers such as IL-6 and IL-9 at CS30, when comparing critical and non-critical cases, may be associated with the symptoms reported by individuals with long COVID-19.[54,55]

In summary, this study highlights proteins associated with COVID-19 and reveals distinct pathway and process alterations between patients presenting clinical deterioration (critically ill) and clinical recovery (non-critically ill patients). Metabolic changes, including a shift from OXPHOS to glycolysis, were observed, indicating a rapid infection response accompanied by increased macrophage activation, antigen presentation, phagocytosis, ROS and NO production, as well as the release of immature cells (LDNs). Notably, patients progressing to critical illness showed significantly low-abundance proteins in the PPP and glycolysis pathway compared with those who recovered. Furthermore, this study also emphasized the importance of longitudinal cellular proteomic studies to discover disease progression-related pathways and protein changes that persist even after hospital discharge.

Limitations of the study

This study has some limitations. First, it is a unicentric study and lacks a validation cohort, for example, from another hospital in another region. Nevertheless, this hospital assists a large number of populations in São Paulo, the largest city in Brazil, and may be representative of moderately ill patients usually admitted to hospital wards. Second, this study lacks functional assays to validate the proteome metabolism changes or the potential contribution of the LDNs in our results. We have tried to overcome these limitations by reanalyzing public proteomic datasets.

Despite the limitations, this study has notable strengths. PBMCs are a type of cells not often explored in COVID-19 proteomics. All patients with COVID-19 and HVs are non-vaccinated due to the unavailability of vaccines at the time of enrollment. Evaluating samples obtained during hospitalization and after hospital discharge allowed us to have a broad view of the cellular proteomic alterations during the clinical course of the disease and convalescence.

STAR★METHODS

Detailed methods are provided in the online version of this paper and include the following:

- KEY RESOURCES TABLE
- RESOURCE AVAILABILITY
  - Lead contact
  - Materials availability
  - Data and code availability
- EXPERIMENTAL MODEL AND STUDY PARTICIPANT DETAILS
  - Ethics
  - Sample collection
- METHOD DETAILS
  - Plasma levels of cytokines and proteins related to endothelial-cell interactions and inflammation
  - Preparation of PBMCs and protein extraction and digestion

- TMT labeling
- LC-MS/MS analysis

- QUANTIFICATION AND STATISTICAL ANALYSIS
  - Epidemiologic, clinical, and routine laboratory statistical analysis
  - Proteomic data processing
  - Batch effect correction
  - Differential protein abundance analysis
  - Pathway enrichment analysis
  - Construction and visualization of protein-protein interaction network
  - Temporal proteomic changes
  - Publicly available dataset

SUPPLEMENTAL INFORMATION

Supplemental information can be found online at https://doi.org/10.1016/j.isci.2023.107824.

ACKNOWLEDGMENTS

We thank Eric B. Dammer, Ph.D., Emory University, for providing valuable information on batch correction for proteomic data. We thank Nancy Bellei, Universidade Federal de São Paulo, for the SARS-CoV-2 PCR test. We thank Jackeline Y. Hayashi and Jackson Gabriel Miyamoto, Universidade Federal de São Paulo, for assisting in the standardization of sample preparation. We thank Professors Paolo Di Mascio and Graziella E. Ronsein for the mass spectrometry analyses performed at the Redox Proteomics Core of the Mass Spectrometry Resource at Chemistry Institute, University of São Paulo (FAPESP grant numbers 2012/12663-1 and 2016/00696-3, CEPID Redoxoma 2013/07937-8). This work was funded by FAPESP (Grants 2017/21052-0 and 2020/05110-2) to R.S. G.G.F.L. has a scholarship from FAPESP (2019/20532-3).

AUTHOR CONTRIBUTIONS

G.G.F.L.: Data analysis, curation and visualization, methodology, writing, and review. M.K.C.B.: Flow cytometry, data acquisition and review. P.M.P-P., P.R., A.F., and J.S.O-A.: Study design and selection, enrollment, and monitoring of patients. E.C-N.: Bioinformatics platform support for analysis and review. B.L.F.: Standardization of proteomic sample preparation and review. A.K.T. and G.E.R.: Mass spectrometry-based data acquisition and review. R.S.: Supervision, conceptualization, writing, and review. All authors contributed to the article and approved the submitted version. The graphical abstract was created with BioRender.com.

DECLARATION OF INTERESTS

The authors declare that they have no known competing financial interests or personal relationships that could have appeared to influence the work reported in this paper.

INCLUSION AND DIVERSITY

One or more of the authors of this paper self-identifies as living with a disability. We support inclusive, diverse, and equitable conduct of research.

Received: April 11, 2023
Revised: July 16, 2023
Accepted: August 31, 2023
Published: September 2, 2023

REFERENCES

1. Haldane, V., De Foo, C., Abdalla, S.M., Jung, A.-S., Tan, M., Wu, S., Chua, A., Verma, M., Shrestha, P., Singh, S., et al. (2021). Health systems resilience in managing the COVID-19 pandemic: lessons from 28 countries. Nat. Med. *27*, 964–980. https://doi.org/10.1038/s41591-021-01381-y.
2. Dhama, K., Khan, S., Tiwari, R., Sircar, S., Bhat, S., Malik, Y.S., Singh, K.P., Chaicumpa, W., Bonilla-Aldana, D.K., and Rodriguez-Morales, A.J. (2020). Coronavirus Disease 2019-COVID-19. Clin. Microbiol. Rev. *33*, e00028-20. https://doi.org/10.1128/cmr.00028-20.
3. McElvaney, O.J., McEvoy, N.L., McElvaney, O.F., Carroll, T.P., Murphy, M.P., Dunlea, D.M., Ní Choileáin, O., Clarke, J., O'Connor, E., Hogan, G., et al. (2020). Characterization of the Inflammatory Response to Severe COVID-19 Illness. Am. J. Respir. Crit. Care Med. *202*, 812–821. https://doi.org/10.1164/rccm.202005-1583OC.
4. Tang, N., Li, D., Wang, X., and Sun, Z. (2020). Abnormal coagulation parameters are associated with poor prognosis in patients with novel coronavirus pneumonia. J. Thromb. Haemost. *18*, 844–847. https://doi.org/10.1111/jth.14768.
5. COVID-19 Treatment Guidelines Panel. Coronavirus Disease 2019 (COVID-19) Treatment Guidelines. National Institutes of Health. https://www.covid19treatmentguidelines.nih.gov/.
6. National Institutes of Health. COVID-19 Treatment Guidelines Panel. Coronavirus Disease 2019 (COVID-19) Treatment Guidelines. https://www.covid19treatmentguidelines.nih.gov/.
7. Nalbandian, A., Sehgal, K., Gupta, A., Madhavan, M.V., McGroder, C., Stevens, J.S., Cook, J.R., Nordvig, A.S., Shalev, D., Sehrawat, T.S., et al. (2021). Post-acute

COVID-19 syndrome. Nat. Med. *27*, 601–615. https://doi.org/10.1038/s41591-021-01283-z.

8. Demichev, V., Tober-Lau, P., Lemke, O., Nazarenko, T., Thibeault, C., Whitwell, H., Röhl, A., Freiwald, A., Szyrwiel, L., Ludwig, D., et al. (2021). A time-resolved proteomic and prognostic map of COVID-19. Cell Syst. *12*, 780–794.e7. https://doi.org/10.1016/j.cels.2021.05.005.
9. Shu, T., Ning, W., Wu, D., Xu, J., Han, Q., Huang, M., Zou, X., Yang, Q., Yuan, Y., Bie, Y., et al. (2020). Plasma Proteomics Identify Biomarkers and Pathogenesis of COVID-19. Immunity *53*, 1108–1122.e5. https://doi.org/10.1016/j.immuni.2020.10.008.
10. Ahern, D.J., Ai, Z., Ainsworth, M., Allan, C., Allcock, A., Angus, B., Ansari, M.A., Arancibia-Cárcamo, C.V., Aschenbrenner, D., Attar, M., et al. (2022). A blood atlas of COVID-19 defines hallmarks of disease severity and specificity. Cell *185*, 916–938.e58. https://doi.org/10.1016/j.cell.2022.01.012.
11. Captur, G., Moon, J.C., Topriceanu, C.-C., Joy, G., Swadling, L., Hallqvist, J., Doykov, I., Patel, N., Spiewak, J., Baldwin, T., et al. (2022). Plasma proteomic signature predicts who will get persistent symptoms following SARS-CoV-2 infection. EBioMedicine *85*, 104293. https://doi.org/10.1016/j.ebiom.2022.104293.
12. Overmyer, K.A., Shishkova, E., Miller, I.J., Balnis, J., Bernstein, M.N., Peters-Clarke, T.M., Meyer, J.G., Quan, Q., Muehlbauer, L.K., Trujillo, E.A., et al. (2021). Large-Scale Multi-omic Analysis of COVID-19 Severity. Cell Syst. *12*, 23–40.e7. https://doi.org/10.1016/j.cels.2020.10.003.
13. Li, J., Guo, M., Tian, X., Wang, X., Yang, X., Wu, P., Liu, C., Xiao, Z., Qu, Y., Yin, Y., et al. (2021). Virus-Host Interactome and Proteomic Survey Reveal Potential Virulence Factors Influencing SARS-CoV-2 Pathogenesis. Méd. *2*, 99–112.e7. https://doi.org/10.1016/j.medj.2020.07.002.
14. Carapito, R., Li, R., Helms, J., Carapito, C., Gujja, S., Rolli, V., Guimaraes, R., Malagon-Lopez, J., Spinnhirny, P., Lederle, A., et al. (2022). Identification of driver genes for critical forms of COVID-19 in a deeply phenotyped young patient cohort. Sci. Transl. Med. *14*, eabj7521. https://doi.org/10.1126/scitranslmed.abj7521.
15. Veglia, F., Sanseviero, E., and Gabrilovich, D.I. (2021). Myeloid-derived suppressor cells in the era of increasing myeloid cell diversity. Nat. Rev. Immunol. *21*, 485–498. https://doi.org/10.1038/s41577-020-00490-y.
16. Park, S.J., Nam, D.E., Seong, H.C., and Hahn, Y.S. (2022). New Discovery of Myeloid-Derived Suppressor Cell's Tale on Viral Infection and COVID-19. Front. Immunol. *13*, 842535. https://doi.org/10.3389/fimmu.2022.842535.
17. Sen, P., Kemppainen, E., and Orešič, M. (2017). Perspectives on Systems Modeling of Human Peripheral Blood Mononuclear Cells. Front. Mol. Biosci. *4*, 96. https://doi.org/10.3389/fmolb.2017.00096.
18. Peçanha-Pietrobom, P.M., Leite, G.G.F., Hunter, J., Ferreira, P.R.A., Burattini, M.N., Bellei, N., Ota-Arakaki, J.S., and Salomao, R. (2021). The clinical course of hospitalized moderately ill COVID-19 patients is mirrored by routine hematologic tests and influenced by renal transplantation. PLoS One *16*, e0258987. https://doi.org/10.1371/journal.pone.0258987.
19. Gonçalves, A.N.A., Lever, M., Russo, P.S.T., Gomes-Correia, B., Urbanski, A.H., Pollara, G., Noursadeghi, M., Maracaja-Coutinho, V., and Nakaya, H.I. (2019). Assessing the Impact of Sample Heterogeneity on Transcriptome Analysis of Human Diseases Using MDP Webtool. Front. Genet. *10*, 971. https://doi.org/10.3389/fgene.2019.00971.
20. Leite, G.G.F., Ferreira, B.L., Tashima, A.K., Nishiduka, E.S., Cunha-Neto, E., Brunialti, M.K.C., Assuncao, M., Azevedo, L.C.P., Freitas, F., van der Poll, T., et al. (2021). Combined Transcriptome and Proteome Leukocyte's Profiling Reveals Up-Regulated Module of Genes/Proteins Related to Low Density Neutrophils and Impaired Transcription and Translation Processes in Clinical Sepsis. Front. Immunol. *12*, 744799. https://doi.org/10.3389/fimmu.2021.744799.
21. Eisfeld, A.J., Halfmann, P.J., Wendler, J.P., Kyle, J.E., Burnum-Johnson, K.E., Peralta, Z., Maemura, T., Walters, K.B., Watanabe, T., Fukuyama, S., et al. (2017). Multi-platform 'Omics Analysis of Human Ebola Virus Disease Pathogenesis. Cell Host Microbe *22*, 817–829.e8. https://doi.org/10.1016/j.chom.2017.10.011.
22. Mukund, K., Nayak, P., Ashokkumar, C., Rao, S., Almeda, J., Betancourt-Garcia, M.M., Sindhi, R., and Subramaniam, S. (2021). Immune Response in Severe and Non-Severe Coronavirus Disease 2019 (COVID-19) Infection: A Mechanistic Landscape. Front. Immunol. *12*, 738073. https://doi.org/10.3389/fimmu.2021.738073.
23. Huang, C., Wang, Y., Li, X., Ren, L., Zhao, J., Hu, Y., Zhang, L., Fan, G., Xu, J., Gu, X., et al. (2020). Clinical features of patients infected with 2019 novel coronavirus in Wuhan, China. Lancet *395*, 497–506. https://doi.org/10.1016/s0140-6736(20)30183-5.
24. Wang, Z., Yang, B., Li, Q., Wen, L., and Zhang, R. (2020). Clinical Features of 69 Cases With Coronavirus Disease 2019 in Wuhan, China. Clin. Infect. Dis. *71*, 769–777. https://doi.org/10.1093/cid/ciaa272.
25. Lieberman, N.A.P., Peddu, V., Xie, H., Shrestha, L., Huang, M.L., Mears, M.C., Cajimat, M.N., Bente, D.A., Shi, P.Y., Bovier, F., et al. (2020). In vivo antiviral host transcriptional response to SARS-CoV-2 by viral load, sex, and age. PLoS Biol. *18*, e3000849. https://doi.org/10.1371/journal.pbio.3000849.
26. Song, J.W., Lam, S.M., Fan, X., Cao, W.J., Wang, S.Y., Tian, H., Chua, G.H., Zhang, C., Meng, F.P., Xu, Z., et al. (2020). Omics-Driven Systems Interrogation of Metabolic Dysregulation in COVID-19 Pathogenesis. Cell Metabol. *32*, 188–202.e5. https://doi.org/10.1016/j.cmet.2020.06.016.
27. Guarnieri, J.W., Dybas, J.M., Fazelinia, H., Kim, M.S., Frere, J., Zhang, Y., Albrecht, Y.S., Murdock, D.G., Angelin, A., Singh, L.N., et al. (2022). Targeted Down Regulation Of Core Mitochondrial Genes During SARS-CoV-2 Infection. Preprint at bioRxiv. https://doi.org/10.1101/2022.02.19.481089.
28. Ambikan, A.T., Yang, H., Krishnan, S., Svensson Akusjärvi, S., Gupta, S., Lourda, M., Sperk, M., Arif, M., Zhang, C., Nordqvist, H., et al. (2022). Multi-omics personalized network analyses highlight progressive disruption of central metabolism associated with COVID-19 severity. Cell Syst. *13*, 665–681.e4. https://doi.org/10.1016/j.cels.2022.06.006.
29. Krishnan, S., Nordqvist, H., Ambikan, A.T., Gupta, S., Sperk, M., Svensson-Akusjärvi, S., Mikaeloff, F., Benfeitas, R., Saccon, E., Ponnan, S.M., et al. (2021). Metabolic Perturbation Associated With COVID-19 Disease Severity and SARS-CoV-2 Replication. Mol. Cell. Proteomics *20*, 100159. https://doi.org/10.1016/j.mcpro.2021.100159.
30. Yaneske, E., Zampieri, G., Bertoldi, L., Benvenuto, G., and Angione, C. (2021). Genome-scale metabolic modelling of SARS-CoV-2 in cancer cells reveals an increased shift to glycolytic energy production. FEBS Lett. *595*, 2350–2365. https://doi.org/10.1002/1873-3468.14180.
31. Ferreira, B.L., Sousa, M.B., Leite, G.G.F., Brunialti, M.K.C., Nishiduka, E.S., Tashima, A.K., van der Poll, T., and Salomão, R. (2022). Glucose metabolism is upregulated in the mononuclear cell proteome during sepsis and supports endotoxin-tolerant cell function. Front. Immunol. *13*, 1051514. https://doi.org/10.3389/fimmu.2022.1051514.
32. Cheng, S.-C., Scicluna, B.P., Arts, R.J.W., Gresnigt, M.S., Lachmandas, E., Giamarellos-Bourboulis, E.J., Kox, M., Manjeri, G.R., Wagenaars, J.A.L., Cremer, O.L., et al. (2016). Broad defects in the energy metabolism of leukocytes underlie immunoparalysis in sepsis. Nat. Immunol. *17*, 406–413. https://doi.org/10.1038/ni.3398.
33. O'Neill, L.A.J., Kishton, R.J., and Rathmell, J. (2016). A guide to immunometabolism for immunologists. Nat. Rev. Immunol. *16*, 553–565. https://doi.org/10.1038/nri.2016.70.
34. Nunn, A.V.W., Guy, G.W., Brysch, W., and Bell, J.D. (2022). Understanding Long COVID; Mitochondrial Health and Adaptation-Old Pathways, New Problems. Biomedicines *10*, 3113. https://doi.org/10.3390/biomedicines10123113.
35. Davis, H.E., McCorkell, L., Vogel, J.M., and Topol, E.J. (2023). Long COVID: major findings, mechanisms and recommendations. Nat. Rev. Microbiol. *21*, 133–146. https://doi.org/10.1038/s41579-022-00846-2.
36. Britt, E.C., Lika, J., Giese, M.A., Schoen, T.J., Seim, G.L., Huang, Z., Lee, P.Y., Huttenlocher, A., and Fan, J. (2022). Switching to the cyclic pentose phosphate pathway powers the oxidative burst in activated neutrophils. Nat. Metab. *4*, 389–403. https://doi.org/10.1038/s42255-022-00550-8.
37. Kuehne, A., Emmert, H., Soehle, J., Winnefeld, M., Fischer, F., Wenck, H., Gallinat, S., Terstegen, L., Lucius, R., Hildebrand, J., and Zamboni, N. (2015). Acute Activation of Oxidative Pentose Phosphate Pathway as First-Line Response to Oxidative Stress in Human Skin Cells. Mol. Cell *59*, 359–371. https://doi.org/10.1016/j.molcel.2015.06.017.
38. Nabavi, S.F., Habtemariam, S., Sureda, A., Banach, M., Berindan-Neagoe, I., Cismaru, C.A., Bagheri, M., Bagheri, M.S., and Nabavi, S.M. (2020). Glucose-6-phosphate dehydrogenase deficiency and SARS-CoV-2 mortality: Is there a link and what should we do? Clin. Biochem. *86*, 31–33. https://doi.org/10.1016/j.clinbiochem.2020.09.004.
39. Mahrooz, A., Muscogiuri, G., Buzzetti, R., and Maddaloni, E. (2021). The complex combination of COVID-19 and diabetes: pleiotropic changes in glucose metabolism. Endocrine *72*, 317–325. https://doi.org/10.1007/s12020-021-02729-7.
40. Littera, R., Campagna, M., Deidda, S., Angioni, G., Cipri, S., Melis, M., Firinu, D., Santus, S., Lai, A., Porcella, R., et al. (2020).

Human Leukocyte Antigen Complex and Other Immunogenetic and Clinical Factors Influence Susceptibility or Protection to SARS-CoV-2 Infection and Severity of the Disease Course. The Sardinian Experience. Front. Immunol. *11*, 605688. https://doi.org/10.3389/fimmu.2020.605688.

41. Buinitskaya, Y., Gurinovich, R., Wlodaver, C.G., and Kastsiuchenka, S. (2020). Centrality of G6PD in COVID-19: The Biochemical Rationale and Clinical Implications. Front. Med. *7*, 584112. https://doi.org/10.3389/fmed.2020.584112.
42. Zhang, D., Zhu, L., Wang, Y., Li, P., and Gao, Y. (2022). Translational Control of COVID-19 and Its Therapeutic Implication. Front. Immunol. *13*, 857490. https://doi.org/10.3389/fimmu.2022.857490.
43. Finkel, Y., Gluck, A., Nachshon, A., Winkler, R., Fisher, T., Rozman, B., Mizrahi, O., Lubelsky, Y., Zuckerman, B., Slobodin, B., et al. (2021). SARS-CoV-2 uses a multipronged strategy to impede host protein synthesis. Nature *594*, 240–245. https://doi.org/10.1038/s41586-021-03610-3.
44. Banerjee, A.K., Blanco, M.R., Bruce, E.A., Honson, D.D., Chen, L.M., Chow, A., Bhat, P., Ollikainen, N., Quinodoz, S.A., Loney, C., et al. (2020). SARS-CoV-2 Disrupts Splicing, Translation, and Protein Trafficking to Suppress Host Defenses. Cell *183*, 1325–1339.e21. https://doi.org/10.1016/j.cell.2020.10.004.
45. Hassani, M., Hellebrekers, P., Chen, N., van Aalst, C., Bongers, S., Hietbrink, F., Koenderman, L., and Vrisekoop, N. (2020). On the origin of low-density neutrophils. J. Leukoc. Biol. *107*, 809–818. https://doi.org/10.1002/jlb.5hr0120-459r.
46. Morrissey, S.M., Geller, A.E., Hu, X., Tieri, D., Ding, C., Klaes, C.K., Cooke, E.A., Woeste, M.R., Martin, Z.C., Chen, O., et al. (2021). A specific low-density neutrophil population correlates with hypercoagulation and disease severity in hospitalized COVID-19 patients. JCI Insight *6*, e148435. https://doi.org/10.1172/jci.insight.148435.
47. Johansson, C., and Kirsebom, F.C.M. (2021). Neutrophils in respiratory viral infections. Mucosal Immunol. *14*, 815–827. https://doi.org/10.1038/s41385-021-00397-4.
48. Elahi, S. (2022). Hematopoietic responses to SARS-CoV-2 infection. Cell. Mol. Life Sci. *79*, 187. https://doi.org/10.1007/s00018-022-04220-6.
49. Dienz, O., Rud, J.G., Eaton, S.M., Lanthier, P.A., Burg, E., Drew, A., Bunn, J., Suratt, B.T., Haynes, L., and Rincon, M. (2012). Essential role of IL-6 in protection against H1N1 influenza virus by promoting neutrophil survival in the lung. Mucosal Immunol. *5*, 258–266. https://doi.org/10.1038/mi.2012.2.
50. Kothari, N., Keshari, R.S., Bogra, J., Kohli, M., Abbas, H., Malik, A., Dikshit, M., and Barthwal, M.K. (2011). Increased myeloperoxidase enzyme activity in plasma is an indicator of inflammation and onset of sepsis. J. Crit. Care *26*, 435.e1–435.e7. https://doi.org/10.1016/j.jcrc.2010.09.001.
51. Zhang, Y., Wang, Y., Wu, W., Liu, P., Sun, S., Hong, M., Yuan, Y., Xia, Q., and Chen, Z. (2022). Elevation of neutrophil carcinoembryonic antigen-related cell adhesion molecule 1 associated with multiple inflammatory mediators was related to different clinical stages in ischemic stroke patients. J. Clin. Lab. Anal. *36*, e24526. https://doi.org/10.1002/jcla.24526.
52. Glowinska, B., Urban, M., Peczynska, J., and Florys, B. (2005). Soluble adhesion molecules (sICAM-1, sVCAM-1) and selectins (sE selectin, sP selectin, sL selectin) levels in children and adolescents with obesity, hypertension, and diabetes. Metabolism *54*, 1020–1026. https://doi.org/10.1016/j.metabol.2005.03.004.
53. Xiao, N., Nie, M., Pang, H., Wang, B., Hu, J., Meng, X., Li, K., Ran, X., Long, Q., Deng, H., et al. (2021). Integrated cytokine and metabolite analysis reveals immunometabolic reprogramming in COVID-19 patients with therapeutic implications. Nat. Commun. *12*, 1618. https://doi.org/10.1038/s41467-021-21907-9.
54. Kappelmann, N., Dantzer, R., and Khandaker, G.M. (2021). Interleukin-6 as potential mediator of long-term neuropsychiatric symptoms of COVID-19. Psychoneuroendocrinology *131*, 105295. https://doi.org/10.1016/j.psyneuen.2021.105295.
55. Schultheiß, C., Willscher, E., Paschold, L., Gottschick, C., Klee, B., Henkes, S.S., Bosurgi, L., Dutzmann, J., Sedding, D., Frese, T., et al. (2022). The IL-1β, IL-6, and TNF cytokine triad is associated with post-acute sequelae of COVID-19. Cell Rep. Med. *3*, 100663. https://doi.org/10.1016/j.xcrm.2022.100663.
56. da Saúde, M.. Orientações Para Manejo De Pacientes Com Covid-19. https://bvsms.saude.gov.br/bvs/publicacoes/manejo_clinico_covid-19_atencao_especializada.pdf.
57. Bradford, M.M. (1976). A rapid and sensitive method for the quantitation of microgram quantities of protein utilizing the principle of protein-dye binding. Anal. Biochem. *72*, 248–254. https://doi.org/10.1016/0003-2697(76)90527-3.
58. Maes, E., Valkenborg, D., Baggerman, G., Willems, H., Landuyt, B., Schoofs, L., and Mertens, I. (2015). Determination of Variation Parameters as a Crucial Step in Designing TMT-Based Clinical Proteomics Experiments. PLoS One *10*, e0120115. https://doi.org/10.1371/journal.pone.0120115.
59. Balestra, A.C., Zeeshan, M., Rea, E., Pasquarello, C., Brusini, L., Mourier, T., Subudhi, A.K., Klages, N., Arboit, P., Pandey, R., et al. (2020). A divergent cyclin/cyclin-dependent kinase complex controls the atypical replication of a malaria parasite during gametogony and transmission. Elife *9*, e56474. https://doi.org/10.7554/eLife.56474.
60. Kumar, V., Ray, S., Ghantasala, S., and Srivastava, S. (2020). An Integrated Quantitative Proteomics Workflow for Cancer Biomarker Discovery and Validation in Plasma. Front. Oncol. *10*, 543997. https://doi.org/10.3389/fonc.2020.543997.
61. Voß, H., Schlumbohm, S., Barwikowski, P., Wurlitzer, M., Dottermusch, M., Neumann, P., Schlüter, H., Neumann, J.E., and Krisp, C. (2022). HarmonizR enables data harmonization across independent proteomic datasets with appropriate handling of missing values. Nat. Commun. *13*, 3523. https://doi.org/10.1038/s41467-022-31007-x.
62. Wei, R., Wang, J., Su, M., Jia, E., Chen, S., Chen, T., and Ni, Y. (2018). Missing Value Imputation Approach for Mass Spectrometry-based Metabolomics Data. Sci. Rep. *8*, 663. https://doi.org/10.1038/s41598-017-19120-0.
63. Gutierrez-Quiceno, L., Dammer, E.B., Johnson, A.G., Webster, J.A., Shah, R., Duong, D., Yin, L., Seyfried, N.T., Alvarez, V.E., Stein, T.D., et al. (2021). A proteomic network approach resolves stage-specific molecular phenotypes in chronic traumatic encephalopathy. Mol. Neurodegener. *16*, 40. https://doi.org/10.1186/s13024-021-00462-3.
64. Kumar, L., and E Futschik, M. (2007). Mfuzz: a software package for soft clustering of microarray data. Bioinformation *2*, 5–7. https://doi.org/10.6026/97320630002005.
65. Haering, M., and Habermann, B.H. (2021). RNfuzzyApp: an R shiny RNA-seq data analysis app for visualisation, differential expression analysis, time-series clustering and enrichment analysis. F1000Res. *10*, 654. https://doi.org/10.12688/f1000research.54533.2.

STAR★METHODS

KEY RESOURCES TABLE

REAGENT or RESOURCE	SOURCE	IDENTIFIER
Chemicals, peptides, and recombinant proteins		
Methanol	Sigma-Aldrich	Cat# 34860
Acetonitrile	Sigma-Aldrich	Cat# 34851
DL-Dithiothreitol	Sigma-Aldrich	Cat# D0632
Iodoacetamide	Sigma-Aldrich	Cat# I1149
Trypsin/Lys-C Mix	Promega	Cat# V5071
50% Hydroxylamine for TMT experiments	Thermo Scientific	Cat# 90115
Urea	Sigma-Aldrich	Cat# 51456
Thiourea	Sigma-Aldrich	Cat# T8656
Protease Inhibitor Mix	Cytiva	Cat# GE80-6501-23
1M Triethylammonium bicarbonate (TEAB) for TMT experiments	Thermo Scientific	Cat# 90114
PolyLC C18 tips	PolyLC Inc	Cat# TT200C18.96
Critical commercial assays		
Pierce™ BCA Protein Assay Kits	Thermo Scientific	Cat# 23225
Pierce™ Quantitative Peptide Assays	Thermo Scientific	Cat# 23275
TMTsixplex™ Isobaric Label Reagent	Thermo Scientific	Cat# 90066
Deposited data		
Mass spectrometry data	This paper	PXD040245
Mass spectrometry data	Carapito et al.[14]	PXD025265
Software and algorithms		
R software environment (version 4.2.0)	R Project	https://www.r-project.org
SPSS Statistics software (version 21)	IBM	https://www.ibm.com/
UniProt database	UniProt Consortium	https://www.uniprot.org/
Perseus (version 2.0.6.0)	MaxQuant	https://maxquant.net/perseus/
Ingenuity Pathway Analysis	QIAGEN	https://digitalinsights.qiagen.com/products-overview/discovery-insights-portfolio/analysis-and-visualization/qiagen-ipa/
Proteome Discoverer Suite (version 2.4)	Thermo Scientific	https://www.thermofisher.com/us/en/home.html
Cytoscape (version 3.9.1)	Cytoscape Consortium	https://cytoscape.org/
stringApp (version 1.7.1)	N/A	https://apps.cytoscape.org/apps/stringapp
Omics Visualizer app (version 1.3.0)	N/A	https://apps.cytoscape.org/download/stats/omicsvisualizer/
DAVID Bioinformatics Resources (version 2022q4)	LHRI	https://david.ncifcrf.gov/
LIMMA (version 3.42.2)	Bioconductor	https://bioconductor.org/packages/release/bioc/html/limma.html
Mfuzz (version 2.56.0)	Bioconductor	https://www.bioconductor.org/packages/release/bioc/html/Mfuzz.html

RESOURCE AVAILABILITY

Lead contact

Further information and requests for resources and reagents should be directed to and will be fulfilled by the lead contact, Reinaldo Salomão (rsalomao@unifesp.br).

Materials availability

This study did not generate new unique reagents.

Data and code availability

- Raw and processed mass spectrometry proteomic data generated in this study are available at ProteomeXchange with the dataset identifier PXD040245. The following public proteomic data were downloaded and analyzed in this study: PXD025265.
- This paper does not report original code. The R code used for batch correction can be downloaded from https://github.com/GiuseppeLeite/COVID19_Proteomic.
- Any additional information required to reanalyze the data reported in this work is available from the lead contact upon reasonable request.

EXPERIMENTAL MODEL AND STUDY PARTICIPANT DETAILS

Ethics

This was a prospective cohort study conducted at Hospital São Paulo, which is a tertiary university hospital in São Paulo with approximately 12.3 million inhabitants.[18] The study protocol was approved by the research ethics committee and all volunteers gave written informed consent before enrollment in the cohort (Process number 4.453.137). The study included adult patients (≥ 18 years old) diagnosed with COVID-19 based on positive reverse transcriptase polymerase chain reaction (RT-PCR) results from nasopharynx swabs. They were admitted to the hospital wards between May 10 and September 26, 2020, with moderate to severe illness as defined by National Institutes of Health and World Health Organization guidelines.[5,6] Patients referred to outpatient clinics or admitted to the ICU were excluded. The patients were prospectively followed and classified as critical or non-critical based on their clinical course and need for ICU support.[5,6,56] Out of the initial 68 moderately ill patients in the cohort, 30 were included in the proteomic analysis. One patient was excluded after preliminary analyses (see below). Additionally, 11 healthy volunteers, matched for age and gender, were selected as controls. The healthy volunteers underwent comprehensive clinical evaluation, tested negative for SARS-CoV-2 antibodies, and had negative RT-PCR results from nasopharynx swabs. Sex and ages of human subjects are reported in the current manuscript (Table S1).

Sample collection

Blood samples were collected from patients and HVs in ethylenediaminetetraacetic acid-treated tubes (BD Biosciences, San Diego, CA, USA), and plasma and PBMCs were separated using a Ficoll gradient method (Ficoll-Paque PLUS, GE Healthcare Biosciences, Uppsala, Sweden). Plasma samples were stored at −80°C, and PBMCs were stored in liquid nitrogen before use.

METHOD DETAILS

Plasma levels of cytokines and proteins related to endothelial-cell interactions and inflammation

Circulating levels of cytokines and proteins related to endothelial-cell interactions and inflammation were determined by flow cytometry (LSRFortessa, BD Biosciences, San Diego, CA, USA) using Cytometric Bead Array Flex Set kits (BD Biosciences, San Diego, CA, USA) or the kit MILLIPLEX® MAP Human Cardiovascular Disease (CVD) Magnetic Bead Panel 2 - Cardiovascular Disease Multiplex Assay (Millipore, Temecula, CA, USA) in MAGPIX® Instrument (Luminex Corporation, Austin, TX, USA). Details information on the mediators is shown in Table S19.

Preparation of PBMCs and protein extraction and digestion

Protein samples were prepared as previously described[20] with minor changes. Briefly, PBMCs were thawed, and the protein extracts were obtained by lysis in 7 M urea, 2 M thiourea, and 200 mM Dithiothreitol (DTT, Sigma Aldrich, St. Louis, MO, USA) with the Protease Inhibitor Mix (Cytiva, Marlborough, MA, USA). After centrifugation at 13, 000 g for 15 min at 4°C, the protein concentration in the supernatants was determined using the Bradford method.[57] The samples were reduced with 5 mM DTT at 65°C for 30 min and then alkylated with 15 mM iodoacetamide (Sigma Aldrich, St. Louis, MO, USA) at room temperature for 30 min in the dark. The proteins were precipitated in acetone: methanol (8:1, v:v) at −80°C overnight (16 h) and, after two washes with methanol, recovered by centrifugation at 14, 000 g for 10 min at 4°C. They were then dissolved in 100 mM triethylammonium bicarbonate buffer (TEAB, Thermo Scientific, Waltham, MA, USA) to a protein concentration of 1 $\mu g.\mu L^{-1}$. Trypsin/Lys-C Mix (Promega, Madison, WI, USA) was added at a 1:50 enzyme:protein ratio at 37°C, and samples were digested overnight (16 h). The peptides were then desalted using PolyLC C18 tips (PolyLC Inc., Waltham, MA, USA), vacuum-dried, and stored at −80°C.

TMT labeling

After protein extraction and digestion, the peptides were dissolved in 100 mM of TEAB buffer. The peptide concentrations were measured using Quantitative Colorimetric Peptide Assay (Thermo Scientific, Waltham, MA, USA) before TMT labeling to ensure that the amounts of peptides in each channel for TMT labeling were equal. TMT labelling was performed according to the manufacturer's recommendations with minor modifications. For tag reconstitution, the TMT reagent (TMT sixplex™ Isobaric Label Reagent Set, Thermo Scientific, Waltham, MA, USA) was dissolved in 41 µl acetonitrile (Sigma Aldrich, St. Louis, MO, USA) according to the manufacturer's instructions. Each batch

of the TMT experiment contained five different samples and one global internal standard (GIS) sample created by pooling PBMCs samples from all individuals of the cohort (TMT channel 126 was used to label GIS). From every sample, 25 μg was labeled with 10 μl of a TMT tag. Reactions were incubated at room temperature for 1 h. The labeling reaction was quenched by an additional 4 μl of 5% hydroxylamine for 15 min. The TMT-labeled samples were pooled with a protein concentration ratio of 1:1:1:1:1:1.[58] Each mixture was dried and stored at −20°C until the liquid chromatography coupled to tandem mass spectrometry (LC-MS/MS) analysis.

LC-MS/MS analysis

Samples were analyzed by LC-MS/MS using an Orbitrap Fusion Lumos mass spectrometer (Thermo Scientific, Waltham, MA, USA) coupled to a Nano EASY-nLC 1200 (Thermo Scientific, Waltham, MA, USA). TMT-labeled peptides were injected into a trap column (nanoViper C18, 3 μm, 75 μm × 2 cm, Thermo Scientific, Waltham, MA, USA) with 12 μL of solvent A (0.1% formic acid) at 980 bar. The trapped peptides were eluted onto a C18 column (nanoViper C18, 2 μm, 75 μm × 15 cm) at a flow rate of 300 nL/min and subsequently separated with a 5%–28% acetonitrile gradient with 0.1% formic acid for 80 min, followed by a 28%–40% acetonitrile gradient with 0.1% formic acid for 10 min. The electrospray ionization source was operated in a positive mode, with voltage and temperature being adjusted to 2.1 kV and 300°C, respectively. The mass spectrometer was operated in a data-dependent acquisition mode, with the MS scan in the m/z range of 400–1600 (with a target value of 10^6 ions) using the Orbitrap analyzer at a resolution of 120, 000 (at m/z 400), followed by higher-energy collisional dissociation (set to 38%) of the 10 most intense ions at a resolution of 50, 000. The isolation window for precursor ions was set to 0.7 m/z, the minimum count to trigger MS/MS events was 25, 000 counts per second, and the dynamic exclusion time was set to 60 s.

QUANTIFICATION AND STATISTICAL ANALYSIS

Epidemiologic, clinical, and routine laboratory statistical analysis

Statistical analyses were performed using SPSS Statistics software version 21 (IBM Corp., Armonk, NY, USA). Normal distribution and variance homogeneity of data were assessed using the Shapiro–Wilk test and Levene's tests, respectively. Normally distributed variables were expressed as mean and standard deviation and compared using Student's *t*-test. Non-normally distributed variables were expressed as median and 25th and 75th percentiles and compared using Mann–Whitney U test. Categorical data were compared using the chi-squared test. A p-value < 0.05 was considered statistically significant.

Proteomic data processing

Raw data files from Orbitrap Fusion Lumos were processed using Proteome Discoverer Suite version 2.4 (Thermo Scientific, Waltham, MA, USA, formic acid). Peptides were identified using the SEQUEST HT search engine with the UniProtKB/Swiss-Prot (TaxID = 9606, *Homo sapiens*, 20, 315 sequences) database and a list with common contaminants (245 sequences, downloaded from http://www.coxdocs.org/doku.php?id=maxquant:start_downloads.htm, 03/06/2022). The following search settings were applied: precursor mass tolerance of 10 ppm, fragment ion tolerance of 0.02 Da (MS2 mode), fully tryptic specificity, maximum of two missed cleavages, minimum peptide length of 6 and maximum peptide length of 144, TMT-labeled peptide *N*-terminals and lysines (+229.163 Da), carbamidomethylation of cysteine (+57.021 Da) as a fixed modification, and oxidation of methionine residues (+15.994 Da) as a variable modification. The false discovery rate for proteins, peptides, and peptide spectral matches was set to 1%. TMT reporter ions were matched with a 20 ppm tolerance window, and both unique and razor peptides were considered for quantitation. The abundance was normalized on "Total Peptide Amount" and then scaled with "On Controls Average" (TMT channel 126 was used as a reference, GIS).[59] In this case, it summed the peptide group abundance for each sample, determined the maximum sum for all files, and calculated the normalization factor using the sum of the sample and the maximum sum in all files.[60]

Batch effect correction

The matrix of Proteome Discoverer normalized abundance of TMT reporters was imported into the R software environment (version 4.2.0) and was log2 transformed. Proteins quantified in ≥ 50% of samples were included in subsequent analyses. The filtered data were then imputed by applying six different methods using R packages "randomForest" version 4.7-1.1 (function rfImpute), "impute" version 1.70.0 (function impute.knn), or Perseus 2.0.6.0 (imputation from the normal distribution). The "randomForest" was superior to other methods[61,62] and was selected for further use. Imputation was performed in an unsupervised mode, using 1000 trees in 10 iterations.[61] Subsequently, ComBat (R sva package) was used to remove variability due to multiple batches.[63] All data were subjected to iterative outlier removal using the molecular degree perturbation (MDP) web tool.[19] After MDP analyses, one patient was detected as an outlier and removed from all subsequent analyses (Figure S1).

Differential protein abundance analysis

Differential protein abundance analysis was performed using R/Bioconductor package "Limma" (version 3.42.2). The difference in PBMCs proteome profiling between two different groups was detected using the empirical Bayes moderated *t*-statistics test and the Benjamini-Hochberg corrections was applied for all p-values to calculate the false discovery rates (FDR). Differentially abundant proteins (DAPs) between the two groups had to meet the following criteria: p-value < 0.05 and log2 fold change < -0.26 or > 0.26.

Pathway enrichment analysis

The canonical pathway enrichment analysis was performed in the ingenuity pathway analysis (IPA, Qiagen Bioinformatics, Thermo Scientific, Waltham, MA, USA) as described previously.[20] Briefly, each list of DAPs is analyzed separately to determine the most significantly affected pathways and the predicted state. The statistical significance (*p*-value) was calculated using Fischer's exact test and adjusted for multiple comparisons by Benjamini–Hochberg-adjusted q-values. A Z-score $\geq$ 2 (pathway increased) or $\leq$ −2 (pathway decreased) with a B-H q-value $\leq$ 0.05 was used as the significance cutoff for our analysis.

Construction and visualization of protein-protein interaction network

The COVID-19 protein-protein interaction network (PPIN) was created using the DAPs list of D0, D7, and CS30 compared with HVs. The interactions were derived from the STRING database using the Cytoscape stringApp (version 1.7.1) for *Homo sapiens* with a confidence cutoff score set at 0.4 and no additional interactors. The representation of the log2 fold change variation was created using the Omics Visualizer app (version 1.3.0). The modules were created using Markov clustering as described previously.[20] All analyses were performed using Cytoscape (version 3.9.1).

Temporal proteomic changes

Temporal changes related to patients with COVID-19 were detected using the Mfuzz R package (version 2.56.0).[64] The soft clustering analysis was performed using the protein abundance matrix. The samples were grouped according to the disease progression stage and among the three-time points. The optimal number of clusters was defined using the Elbow method.[65] Core cluster proteins were used for the top 10 REACTOME pathway enrichment analyses using the Database for Annotation, Visualization, and Integrated Discovery (DAVID, version 2022q4).

Publicly available dataset

A publicly available proteomic dataset of PBMCs from patients with COVID-19 was obtained from the ProteomeXchange Consortium (PXD025265).[14] This database was compared with our main findings to validate them. Normalized data was downloaded using the access: Project PXD025265. The data was Log2 transformed, and proteins only identified by side, reverse, and the potential contaminant was removed. We keep only proteins with $\geq$2 peptides matched (one of which was unique). Differential protein abundance analysis was performed using R/Bioconductor package "Limma".